Influence of Cation Na/Ca Ratio on Adsorption in LTA 5A: A Systematic Molecular Simulation Study of Alkane Chain Length

E. García-Pérez,[†] D. Dubbeldam,[‡] T. L. M. Maesen,[§] and S. Calero*,[†]

Department of Physical, Chemical, and Natural Systems, University Pablo de Olavide, Ctra. Utrera km 1, 41013 Sevilla, Spain, Chemical and Biological Engineering Department, Northwestern University, 2145 Sheridan Road, Evanston, Illinois 60208, Chevron, Energy Technology Center, Chevron Way 100, Richmond, California 94802-0627

Received: August 2, 2006; In Final Form: September 8, 2006

Recent adsorption isotherms of *n*-alkanes on Ca,Na-LTA-type zeolite afford development of a force field describing the interactions between calcium and *n*-alkanes in configurational-bias Monte Carlo simulations. The force field of Calero et al. (*J. Am. Chem. Soc.* **2004**, *126*, 11377−11386) is able to accurately describe the adsorption properties of linear alkanes in the sodium form of FAU-type zeolites. Here, we extend upon this type of force field by including calcium-type ions. The force field was fitted to reproduce the calcium and sodium cations positions on LTA 5A and the experimental adsorption properties of *n*-alkanes over all range of temperatures and pressures. This opens up a vast amount of experimental data on LTA 5A, both on adsorption and diffusion. Furthermore, evaluation of half a century of reported *n*-alkane adsorption data on LTA-type zeolites indicates that there are many inconsistencies between the various data sets, possibly as a result of (i) undisclosed calcium and sodium contents, (ii) less than perfect drying of the hygroscopic zeolite, and (iii) coadsorption of contaminants such as vacuum grease. Having obtained our force field, and confirmed its reliability on predictions outside the calibration set, we apply the force field on two "open" problems: (a) the heats of adsorption and Henry coefficient as a function of chain length and (b) the effect of cations in LTA-type zeolites. The molecular simulations shed new light on previous experimental findings, and we provide rationalizations on the molecular level that can be generalized to the class of cage/window-type nanoporous materials.

I. Introduction

LTA-type zeolites epitomize how ubiquitous zeolites have become. These zeolites are consumed in large quantities as water softener in detergents and in horticulture, as desiccant in double glazing, and as selective adsorbents for air separation and alkane isomer separation. Unfortunately, the synthesis of more stable (high silica) LTA-type zeolites has only recently been discovered[1] so that LTA-type zeolites have not had a major impact on catalysis yet. From a scientific point of view, the LTA-type structure is an ideal case study, mainly because the structure is well defined (the positions of the aluminum and the cations are known), the topology is a simple cubic lattice, and there is experimental data on different Ca/Na ratios, cell sizes, and on adsorption and diffusion of alkanes varying from methane up to octadecane. Our main aim is to develop a high-quality force field that reproduces the experimental adsorption data and subsequently make an interpretation of the experimental findings at the molecular level. Up-to-date experiments have been unable to provide the link between macroscopic properties and the positions of the molecules inside the zeolite sample, and here is where the strength of molecular simulations comes into play. The force field developed here afford connecting the location, orientation, and configurations of the molecules with the observed experimental adsorption and diffusion properties for alkanes in a cage/window-type environment.

The structure of Linde type-A (LTA-) zeolite consists of an inner cavity that is large enough for structure changing reactions to take place. Access to this cage is severely restricted so that only relatively small compounds can enter and react, e.g., *n*-paraffins and olefins. The crystallographic unit cell consists of eight large spherical cages (named α-cages) of approximately 1.12 nm interconnected via windows of about 0.41 nm diameter. LTA-type zeolites are often synthesized in their sodium form. The Si/Al ratio is approximately unity with a composition of $[Na_{96}Al_{96}Si_{96}O_{384}]$. The Ca/Na form can be obtained by replacing the sodium with calcium cations in a postsynthesis exchange. The positions of ions are of critical importance. If they are located in the eight-ring windows, they obstruct the diffusion. The difference between the Na form of the LTA-type zeolite and the Ca/Na form is a good illustration.[2] The Ca/Na form (zeolite 5A) has approximately four calcium and four sodium ions per cage. None of the windows are blocked by an ion, and the free diameter of the windows is 4.1 Å. The Na form (zeolite 4A) contains 12 sodiums per cage and 100% of the windows are occupied with an ion, partially blocking the window and therefore reducing the effective window size. Exchange with potassium would reduce the window size further (zeolite 3A).

There is an overwhelming amount of experimental data available on adsorption and diffusion in LTA-type zeolites. Despite the small difference in access size between zeolite 4A and 5A, diffusion coefficients in 4A are 4 orders of magnitude lower than in 5A. Because of the slow adsorption kinetics in 4A, equilibration of adsorption isotherms is problematic, and there is little agreement on what constitutes reliable adsorption and diffusion data. Adsorption characteristics of zeolite 5A

* Corresponding author. E-mail: scaldia@upo.es.
[†] University Pablo de Olavide.
[‡] Northwestern University.
[§] Chevron, Energy Technology Center.

10.1021/jp064971y CCC: $33.50
Published on Web 11/08/2006

depend critically on the Ca/Na ratio, but this ratio is not always known or given. The calcium and sodium positions depend on the pretreatment of the zeolite sample (the rate and conditions during the dehydration/steaming process). For diffusion data, there is the additional problem that the source for discrepancies between different methods for measuring intracrystalline diffusion in zeolites is still unresolved. Recently, a collaborative research project has been initiated, with the aim of making comparative diffusion measurements for selected systems under similar conditions by different experimental techniques.[3]

In view of the known problems associated with the cations in 4A and 5A, the discovery of a synthesis for LTA-type silica (ITQ-29)[1] was a welcome event. Well before LTA-type silica had become experimentally accessible, it had already been studied extensively in silico. Fritzsche et al. studied the diffusion of methane in LTA-type zeolite in great detail.[4−7] Bates et al. simulated the energetics of *n*-alkanes from butane to decane in a variety of different all-silica zeolite structures including LTA.[8] Demontis and Suffritti investigated how the sorbate loading controls the diffusion of spherically symmetric Lennard-Jones molecules.[9] Haberlandt discussed diffusion of guest molecules (CH_4, C_2H_6, Xe) in zeolites (LTA-zeolites, silicalite) under different thermodynamic conditions for different intermolecular potentials.[10] The thermal conductivity of model zeolites was investigated using nonequilibrium molecular dynamics calculations by Murashov.[11] Schüring et al. studied the self-diffusion of ethane in cation-free Linde type-A zeolite by molecular dynamics simulations for various temperatures. These simulations predicted that the diffusivity decreases with increasing temperature between 150 and 300 K for a low loading of one molecule per cage.[12] They also developed a random walk treatment of dumb-bell molecules in an LTA zeolite and in chabazite.[13] Dubbeldam et al. simulated self-diffusion coefficients in the range of C_1-C_{24} at various temperatures.[14,15] Tunca and Ford developed a hierarchical approximation of diffusion and adsorption at nonzero loading in microporous materials using methane in LTA as a test system.[16−18] Beerdsen et al. developed a dynamically corrected transition state theory method capable of computing quantitatively the self-diffusivity of adsorbed molecules in confined systems at nonzero loading. For methane and ethane in the model system, LTA perfect agreement with MD was found.[19−21] Demontis et al. studied the equilibrium probability distribution of *N* methane molecules adsorbed in the interior of *n* α-cages of the all-silica LTA-type zeolite.[22] Recently, Beerdsen et al. constructed a classification of pore topologies based on a free energy match between the molecule and the structure of the confinement.[23] They showed that small alkanes in LTA-type zeolites fall into the class of cage-type zeolites, characterized by an initial *increase* in diffusion over loading followed by the usual decrease with loading close to saturation.

In contrast to LTA-type silica, there are precious few papers discussing LTA-type zeolites complete with the usual sodium or calcium cations. Jaramillo and Chandross performed Gibbs ensemble Monte Carlo simulations for the calculation of adsorption of NH_3, CO_2, and H_2O on zeolite 4A.[24] It is clear from the above introduction that, for further advancement, a reliable force field for a LTA-type zeolite with an adjustable Na/Ca ratio is desperately needed. The force field of Calero et al. is able to accurately describe the adsorption properties of linear alkanes in the sodium form of FAU-type zeolites.[25] Here, we extend this force field so as to include calcium cations.

The remainder of this paper is organized as follows. We first describe the choice of the functional forms of the force field, the zeolite A structural details, the final force field parameters, and the simulation methods and details. In the Results Section III, we first show the calibration of the Na/Ca-zeolite parameters by reproducing experimentally known crystallographic positions and occupancies. Next, we show the isotherm set of experimental data along with our fitting results used for calibrating the force field. The section with the results is completed with the predictions of our force field along with available experimental data, i.e., isotherms, heats of adsorption, and Henry coefficients.

II. Methods

A. Force Field Type. The adsorption of hydrocarbons is dominated by dispersion forces. These interactions are notoriously difficult to describe using quantum mechanical approaches. The next level of sophistication is to use an all-atom model. These models are commonly used in the simulations of proteins and other large systems. Given the widespread use of partial atomic charge models, it is important to realize that partial charges cannot be unambiguously assigned to atoms because charge is not an experimentally observable quantity and cannot be unambiguously calculated from the wave function. The united-atom approach circumvents the use of charges. For alkanes in all-silica structures, it was possible to obtain a unique and optimal set of adsorbate−adsorbent parameters.[26,27] The alkane−alkane parameters were taken from refs 28,29. The structure of these types of force field dates back to Kiselev et al.[30] They assumed that oxygen atoms dominate the interactions between the rigid framework and the guest molecules. This type of force field has only two optimization parameters per pseudo-atom, the strength parameter ϵ, and the size parameter σ of the Lennard-Jones potential. Dubbeldam et al. showed that both can be fitted uniquely by using isotherms with inflections.[26] The shape of the inflections are sensitive to size parameter σ, while the amount adsorbed at a particular pressure is dependent on the strength parameter ϵ. It is interesting to note that more elaborate force fields perform worse for adsorption properties in these systems.[27] This misfit reflects the complexity inherent to optimizing a multitude of parameters. Especially, the addition of charge increases the complexity of the approach, for it implies that the uniqueness of the Lennard-Jones parameters is lost. These parameters now have to be retrofitted assuming the chosen charges. With each step of sophistication, e.g., polarization, the parametrization becomes more difficult to link to parameters that can be verified or falsified.

For the limited set of alkane adsorption in microporous silicas, Dubbeldam et al. developed a uniquely parametrized force field. Much more experimental data are available on sodium-containing aluminosilicates. Therefore, Calero et al. extended the force field so as to include sodium ions.[25] In an earlier attempt to include ions into these models, Beerdsen et al.[31,32] were among the first to allow the nonframework cations to move instead of keeping them fixed. In the model of Beerdsen et al.[31,32] and Calero et al.,[25,33] the zeolite and the nonframework cations are assigned partial charges, but the alkanes are still modeled as united atoms. Note that the charges in these works were taken from Jaramillo and Auerbach[34] and the alkane−alkane interactions from Martin et al.[28,29] The charges are also used to represent some average polarization, while the optimization is focused on reproducing the experimentally known crystallographic positions and occupancies of the nonframework cations. The force field of Calero et al. is able to accurately describe the adsorption properties of linear alkanes in the sodium form of FAU-type zeolites.[25] It reproduces the sodium positions in dehydrated FAU-type zeolites known from crystallography

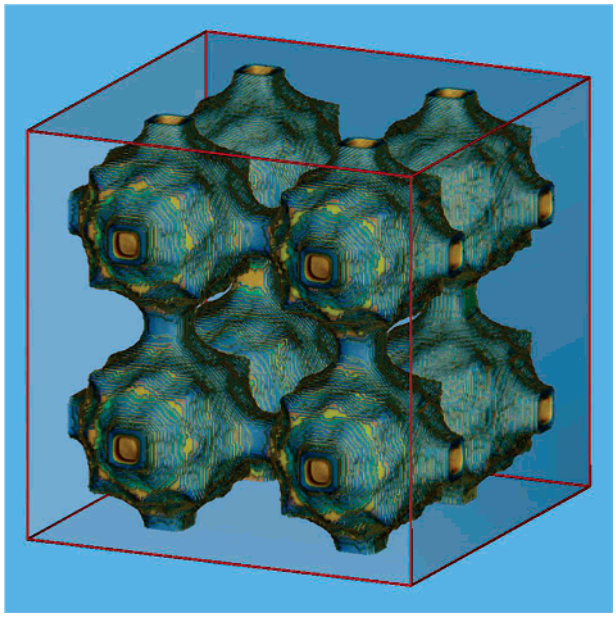

Figure 1. Unit cell of the LTA-type zeolite. The dimensions of the cubic unit cell are around 24−24.5 Å. It contains eight cages connected in a cubic arrangement, and each cage is connected to six other cages by windows of about 5 Å in diameter.

and it predicts how the sodium cations redistribute when *n*-alkanes adsorb. More recent works showed that this force field can be successfully extended to MOR- and MFI-type zeolites.[35−37]

There are many other force fields published in the literature. The consistent valence force field (CVFF) for the adsorption of hydrocarbons in MFI gave a reasonable prediction of the adsorption isotherms.[38] Other examples include the model of June et al.,[39] the AUA model,[40] the models of Vlugt et al.,[41] Smit et al.,[42] and Jaramillo et al.[24,34]

B. LTA-Type Zeolites. The Ca/Na form of the LTA-type structure[43] has a cubic space group $Fm\bar{3}c$ (space group 225), with $a = b = c = 2.4555$ nm and $\alpha = \beta = \gamma = 90°$. The crystallographic unit cell consists of eight large spherical cages (named α-cages) shown in Figure 1. In search of LTA-type zeolites with enough silica to be suited for catalysis, ZK-4 zeolite[44] and zeolite α were reported. However, these remained relatively unstable, for their framework Si/Al ratio remained below 1.7 mol/mol. Consistent with replacing long Al−O bonds by shorter Si−O bonds, the unit cell of such a higher silica LTA-type zeolite shrinks from 24.555 Å for Si/Al = 1 mol/mol to 24.2 Å for Si/Al = 1.67. For recently reported LTA-type silica, the unit cell size is as small as 23.734 Å.[1] LTA-type zeolites obey the Löwenstein rule, i.e., all framework aluminum atoms link via four oxygen atoms to four framework silicon atoms. Because of this strict alternation between aluminum and silicon, capturing the periodicity of the unit cell of LTA-type zeolites with a silicon-to-aluminum ratio of 1 mol/mol requires *two* cages in each direction. There are three types of rings: six-, eight-, and four-membered oxygen rings. The positions of ions are of critical importance if they are located in the windows obstructing the adsorption through the eight-membered oxygen rings. In addition to the relevant cages and channels, there are also topologically disconnected sites. A methane molecule may fit in, e.g., a β (sodalite) cage, but it cannot access such a site from the main (α or super) cages and channels. Accordingly these inaccessible pockets were artificially blocked in our model.

C. Force Field Model and Parameters. The interactions between cations and the zeolite host framework are modeled by Lennard-Jones and Coulomb potentials. The alkane−alkane interactions, alkane−framework interactions, and alkane−cation interactions are modeled by Lennard-Jones potentials only (Table 1). The Coulomb interactions in the system are calculated using the Ewald summation.[45,46] The alkanes are described with a united atom model in which CH_x groups are considered as single interaction centers with their own effective potentials.[47] The beads in the chain are connected by harmonic bonding

TABLE 1: Lennard-Jones Parameters, ϵ/k_B [K] in Top Corner, σ [Å] in Bottom Corner of Each Field, Partial Charges [*e*] of the Framework and the Cations, and the Bond, Bend, and Torsion Potential and Parameters[a]

	O_{Si}	O_{Al}	Si	Al	Na^+	Ca^{2+}	CH_4	CH_3	CH_2
CH_4	115	115			582	590	158.5	130.84	94.21
	3.47	3.47			2.72	2.56	3.72	3.74	3.84
CH_3	93.0	93.0			443	400	130.84	108.0	77.7
	3.48	3.48			2.65	2.6	3.74	3.76	3.86
CH_2	60.5	60.5			310	440	94.21	77.7	56.0
	3.58	3.58			2.95	2.8	3.84	3.86	3.96
Na^+	23.0	23.0					582	443	310
	3.4	3.4					2.72	2.65	2.95
Ca^{2+}	18.0	18.0					590	400	440
	3.45	3.45					2.56	2.6	2.8
charge	$q = -1.025$	$q = -1.2$	$q = +2.05$	$q = +1.75$	$q = +1.0$	$q = +2.0$			
bond	$U^{bond} = {}^1/_2 k_1(r - r_0)^2$								
	$k_1/k_B = 96\,500$ K/Å^2, $r_0 = 1.54$ Å								
bend	$U^{bend} = {}^1/_2 k_2(\cos\theta - \cos\theta_0)^2$								
	$k_2/k_B = 62\,500$ K, $\theta_0 = 114°$								
torsion	$U^{torsion} = \sum_{n=0}^{5} \eta_n \cos^n\phi$								
	$\eta_{n=0\ldots5}/k_B = \{1204.654, 1947.740, -357.845, -1944.666, 715.690, -1565.572\}$								

LJ

$$U_{ij}^{gg,hg,intra} = \begin{cases} 4\epsilon_{ij}\left[\left(\frac{\sigma_{ij}}{r_{ij}}\right)^{12} - \left(\frac{\sigma_{ij}}{r_{ij}}\right)^{6}\right] - E_{cut} & \text{if } r < r_{cut} \\ 0 & \text{if } r \geq r_{cut} \end{cases}$$

[a] The O−CH_x interactions are taken from our previous works,[26,27] O_{Al} are the oxygens bridging one silicon and one aluminum atom, and O_{Si} are oxygens bridging two silicon atoms, $r_{cut} = 12$ [Å] the cutoff distance, and E_{cut} denotes the energy at the cutoff radius (shifted potential).

potentials. The bond bending between three neighboring beads is modeled by a harmonic cosine bending potential, and changes in the torsional angle are controlled by a Ryckaert−Bellemans potential. The beads in a chain separated by more than three bonds interact with each other through a Lennard-Jones potential. The interactions of the adsorbed molecules with the zeolite are dominated by the dispersive forces between the pseudo-atoms and the oxygen atoms of the zeolite,[30,41,48] meaning that the silicon van der Waals interactions are taken into account through an effective potential with only the oxygen atoms.

In the force field described here, an "average" polarization is included implicitly in the parametrization by means of two effects: the polarization induced by the cation on the zeolite and on the alkanes. For the cation−zeolite interactions, we used the approach of Auerbach,[34] taking into account the polarization effects by adjusting the partial charges on the oxygen, depending whether they are connected to Si or Al. Concerning the polarization effects for the cation−alkane interactions, alkanes are very difficult to polarize, and therefore, a logical approach was to use effective Lennard-Jones interactions between the cations and the alkanes.

It should be noted that effective Lennard-Jones potentials implicitly included many-body interactions (polarization), the contributions arising from instantaneous dipole−quadrapole and quadrupole−quadrupole interactions, flexibility of the framework, etc. The flexibility of the framework has been shown to be a minor effect for adsorption of small alkanes.[49]

D. Grand-Canonical Monte Carlo. In adsorption studies, one would like to know the amount of materials adsorbed as a function of pressure and temperature of the reservoir with which the sieve is in contact. Therefore, the natural ensemble to use is the grand-canonical ensemble (or μ, V, T ensemble). In this ensemble, the temperature T, the volume V, and the chemical potential μ are fixed. The equilibrium conditions are that the temperature and chemical potential of the gas inside and outside the adsorbent must be equal. The imposed chemical potential μ can be related to the fugacity, computed directly from the equation of state of the vapor in the reservoir. For all adsorbates, the experimental equation of state is well-known, and we use the Peng−Robinson equation of state to convert the pressure to the corresponding fugacity, introducing only a small correction for the currently studied systems. Another potential issue can arise at very high pressures where measured excess and computed absolute adsorption are not the same. For our systems, the difference is neglectible (smaller than 1%).

The conventional simulation techniques to compute adsorption isotherms are prohibitively expensive for long alkanes. The configurational bias Monte Carlo (CBMC) technique simulates the adsorption isotherms at affordable cost.[50] In a CBMC simulation, chains are grown bead by bead, biasing the growth process toward energetically favorable configurations and avoiding overlap with the zeolite. During the growth, the Rosenbluth factor is calculated. The average Rosenbluth factor is directly related to the excess chemical potential, the free energy, and the Henry coefficient K_H.[46,51] The CBMC algorithm greatly improves the conformational sampling of molecules and increases the efficiency of chain insertions by many orders of magnitude.

E. Simulation Details. The crystallographic positions for the 5A zeolite are taken from Pluth et al.[52] The Si/Al ratio is exactly one, obeying the Löwenstein rule (framework silicon and aluminum strictly alternate). So as to compare with the 5A zeolite used by Ruthven et al., we employed 36 Ca^{2+} and 24 Na^+ per unit cell. To compare with Schirmer et al.,[53] we used 32 Ca^{2+} and 32 Na^+ per unit cell. The simulations were performed using one unit cell with eight cages. Test simulations using $2 \times 2 \times 2$ gave identical results but were deemed too computationally expensive for use with the Ewald summation for all the simulations. The Ewald summation is the most accurate way of computing the Coulomb energy in truly periodic systems, and in all our simulations, the convergence parameter was chosen as $\alpha = 0.3$, with $k = 9$ wave vectors for high accuracy.

TABLE 2: Ca^{2+}−O Distances (Å) in LTA Compared with Firor and Seff,[54] Moon et al.,[55] Jang et al.,[56] Pluth and Smith,[57] and Adams and Haselden[58]

	this work	Firor	Moon	Jang	Pluth	Adams
Ca(I)−O(3)	2.328	2.328	2.224	2.098	2.273	2.287
Ca(II)−O(3)	2.244	2.272	2.307	2.158		2.849
Ca(III)−O(3)	2.273	2.356	2.268	2.265	2.317	
Ca(IV)−O(1)	2.412	3.08				
Ca(IV)−O(2)	2.454	3.0				

Simulations are performed in cycles, and in each cycle, one move is chosen at random with a fixed probability of performing a molecule displacement (10%), rotation around the center of mass (10%), exchange with the reservoir (60%), partial regrowth of a molecule (10%), and a full regrowth at a random position (10%). The maximum translational and rotational displacements are adjusted to achieve an acceptance probability of 50%. The total number of cations remains constant during simulations so only translation movements and regrowth at a random position in the zeolite are considered for this type of particles. The regrowing at a new, randomly selected position bypasses energy barriers and allows for fast equilibration.

For the NVT simulations, the total number of cycles was at least 5×10^5. For the grand-canonical simulations, the number of cycles for isotherms was at least 1×10^6. Note that, in one cycle, one Monte Carlo move is attempted *per particle*. The number of Monte Carlo steps is the number of cycles times the average number of particles. More details on this simulation technique can be found elsewhere.[25−27,41,46]

III. Results

A. Calibration of Zeolite−Ion Interactions. The Na−O interactions were calibrated to reproduce the experimentally known positions in LTA 4A, assuming a charge of $q = +1$ for sodium. Crystallographic studies indicate that these sites are occupied for 97.2, 24.2, and 6.6%, respectively. Molecular simulations with our optimized force field yield occupations of 100, 23.9, and 6.25%, respectively. In addition, the crystallographic locations of the sites obtained through molecular simulations are within 0.2 Å from those obtained though X-ray diffraction. Using this set of parameters derived from this high-alumina LTA-type zeolite, we previously validated the potentials by computing the average sodium−oxygen distances in FAU-type zeolite.[25]

This work uses a realistic description of the interaction between the sodium and calcium cations, the zeolite framework, and the alkanes. We performed simulations to obtain the average calcium−oxygen distances and calcium occupancies in LTA zeolite. The resulting calcium−oxygen distances and calcium occupancies are listed in Tables 2 and 3, respectively.

B. Calibration on Isotherms. Experimentally, measurements of adsorption and diffusion in Ca/Na forms of LTA are challenging. First, there are differences in the Ca/Na cation ratio. In addition, there might be trace of other cations, e.g., potassium, present. Second, diffusion of linear alkanes, especially for the

TABLE 3: Ca site Occupancies in LTA Compared to the Experimental Data of Firor and Seff[54]

	Ca I	Ca II	Ca III	Ca IV
this work	42.1	1.6	4.3	0
exptl data	24	8	8	8

longer ones, is quite slow. This results in very long equilibration times for higher pressures and lower temperatures. Third, Ca/Na forms are highly hydrophilic, so that avoiding water adsorption requires special care. Finally, there are the usual issues when dealing with nanoporous materials: the form of the sample (pellets with binder or crystals), adsorption on the exterior, the quality of the sample, etc. Ideally, one would like to calibrate a force field on various data sets from different authors. From the graphs in the next section, it can be seen that agreement between the various sets is generally only qualitative. We opted for utilizing Ruthven's data as the calibration set because of the large amount of consistent data from a single trustworthy source, obtained through contemporary measurement methods with great care for the quality of the crystal samples. The parameters of methane and ethane could be fitted on the data of Ruthven and co-workers.[59−61] with great accuracy (Figure 2). The overlap of the curves is excellent, i.e., the shape of the isotherms matches at all three temperatures. We have added the isotherm of Loughlin to show that the data for methane are similar but slightly different for different authors. From methane, we obtained the Ca−CH_4 parameter, and from ethane, we obtained Ca−CH_3. The data for propane[59,61,62] is used to obtain Ca−CH_2 and is illustrative for the problems one faces when designing and fitting force fields. First, we note that the data of Grande are different for pellets than for crystals. Obviously, the materials are different, the material based on pellets includes binder, but a correction for the influence of the binder is not trivial. Next, we note that the data of Grande differ from the data of Ruthven, although they are in general agreement. Finally, when fitted on the data of Ruthven, we obtain excellent agreement for 358, 358, and also for 273 K, but *not* for 323 K. Still, there is some support that the simulation data at 323 K might still be correct: the data are consistent, i.e., the spacing over temperature is what you expect, and the simulation data agrees with Grande pellets at 323 K (and extrapolated 423 K).

C. Predictions of Isotherms. Having obtained the Ca−CH_3 parameters from ethane and the Ca−CH_2 parameters from propane, we are able to make predictions for isotherms on longer alkanes and check the validity of the parameters. The data for butane are taken from refs 59, 63, the data for the medium chain length alkanes are taken from refs 64−68, and the data on the longest alkanes reported here are taken from ref 53.

We have plotted the predictions of our force field in Figure 3. For butane, we trace the shape of the curves well, but deviate from the data of Ruthven at the lowest temperatures. The same applies to pentane and hexane and the experimental data of Silva and Rodrigues. However, for heptane, we agree well with Doetsch, for octane, there is remarkable agreement with Vavlitis and Miano, and for decane, we agree very well with Schirmer.[53] We note that the Ca/Na ratio of the samples used by these various authors differ and sometimes are not reported. The adsorption isotherms of long alkanes are plotted in Figure 4. The data of Schirmer are for moderate to high loading. For these loadings, differences between simulation and experiment are to be expected because simulation uses perfect crystals and real samples contain defects. However, for C_{12}, C_{14}, and C_{18}, the difference is systematic and agreement is good.

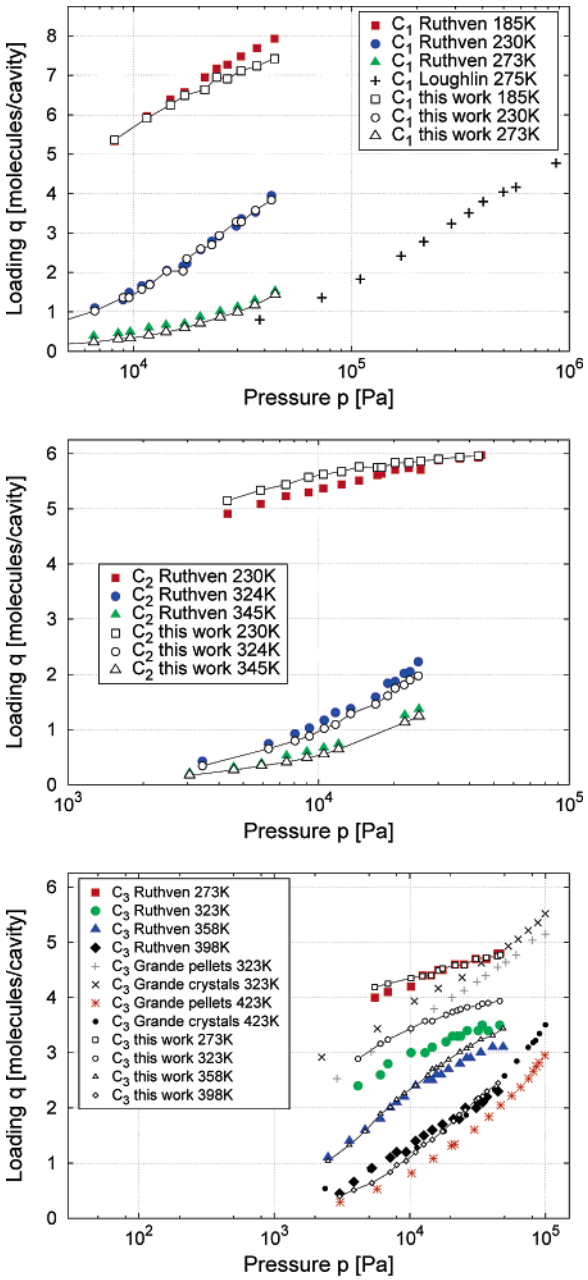

Figure 2. Isotherms of linear alkanes used in the *calibration set* of the force field (top) methane, (middle) ethane, (bottom) propane, in Ca/Na-LTA at various temperatures. Experimental data are taken from Ruthven and co-workers.

D. Predictions of Henry Coefficients and Heats of Adsorption. At low pressures, the loading is linear in pressure with the Henry coefficient as the proportionality constant. A high Henry coefficient means that the zeolite is a strong adsorbent, at least at low loadings. The Henry coefficients for the Ca/Na form and siliceous LTA form obtained from simulation are compared to experimental data in Figure 5. Excellent agreement between the simulations and the experimental data can be observed. Note that the log of the Henry coefficients is not linearly increasing with carbon number. We stress that the Henry coefficients are predictions from our force field and were *not* included in the calibration set. When the log of the Henry coefficients is plotted versus the inverse temperature, two quantities can be obtained: the heat of adsorption as the slope, and the preexponential Henry coefficients as the intersection with the *y*-axis. The heats of adsorption are plotted

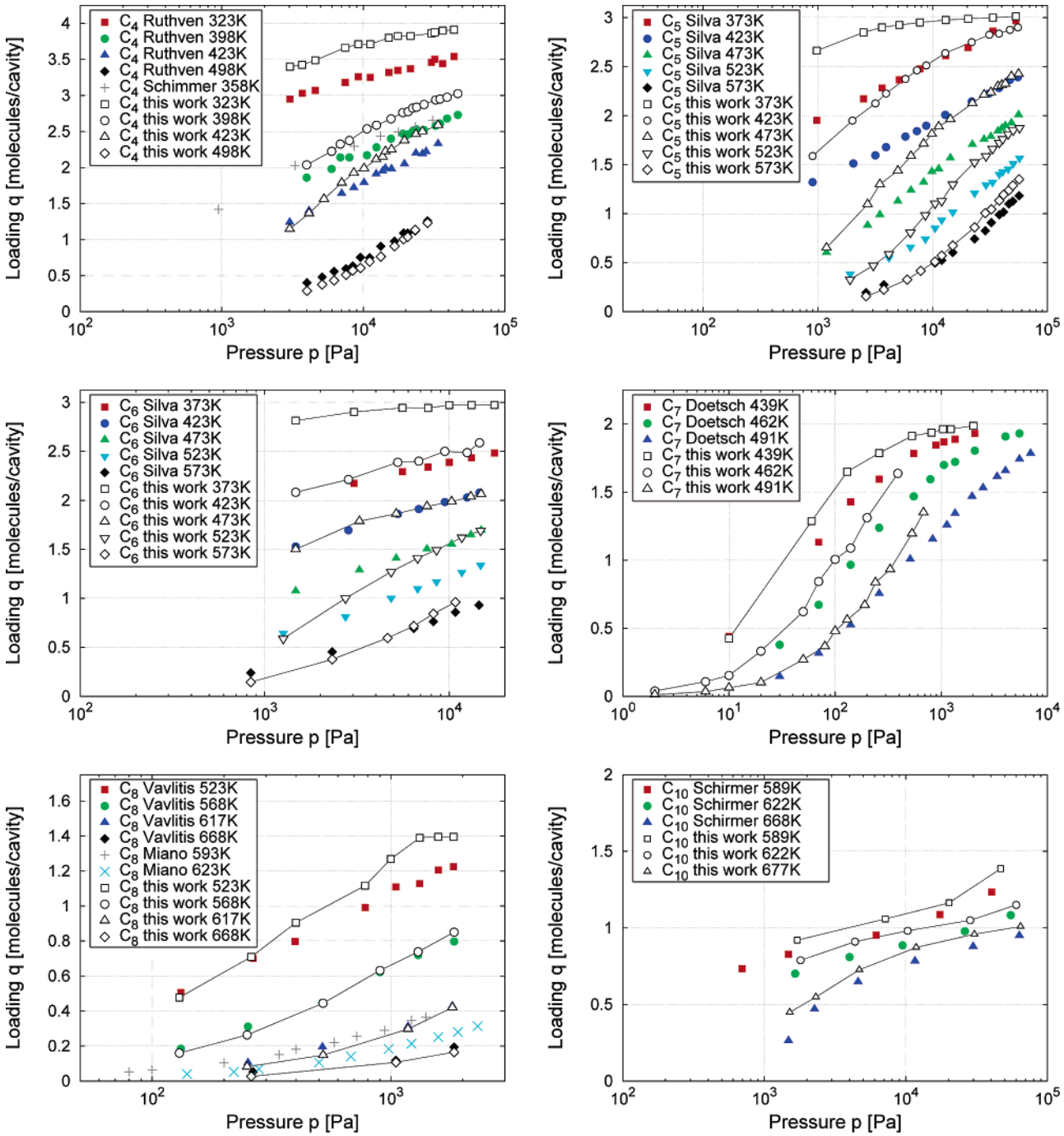

Figure 3. *Predictions* of isotherms of butane to decane compared to various experimental data.

in Figure 6 along with experimental data of Ruthven and other authors. For reference, we have included the simulation data on LTA-type silica with the same unit cell as 5A and for LTA-type silica proper (i.e., with the much smaller unit cell size). The smallest unit cell size yields a better adsorption energy. A single experimental point on LTA-type silica (39 kJ/mol) agrees well with our simulation value (42 kJ/mol). Both are well below the value for zeolite 5A (60 kJ/mol). In Table 4, we have summarized the comparison with the data of Ruthven. The agreement is excellent for heats of adsorption and good for the preexponential Henry coefficients.

The preexponential Henry coefficients for zeolite 5A simulations, LTA-type silica with and without unit cell correction, are plotted in Figure 7. The agreement with Ruthven is good for higher chain lengths. Some interesting effects can be seen here. The simulation shows the expected behavior, a strictly decreasing curve, with the 5A zeolite lower than the other two. Note that the data show two regimes; around $C_{6/7}$, the curves have a different slope. This slope of $\log(K_\infty)$ plotted as a function of carbon number is related to the entropy ΔS per carbon number. Up to medium chain lengths, the chain loses entropy linearly with carbon number compared to the gas phase. As soon as the molecule feels the other side of the cage, the molecule is forced to bend, thereby being even more restricted in freedom.

E. Effect of Cations. An important observation can be made: the difference between zeolite 5A and LTA-type silica becomes many orders of magnitude for increasing chain lengths. The difference becomes even more pronounced at lower temperatures. In Figure 8, we have plotted the adsorption of decane at 300 K by examining the influence of the Ca/Na ratio.

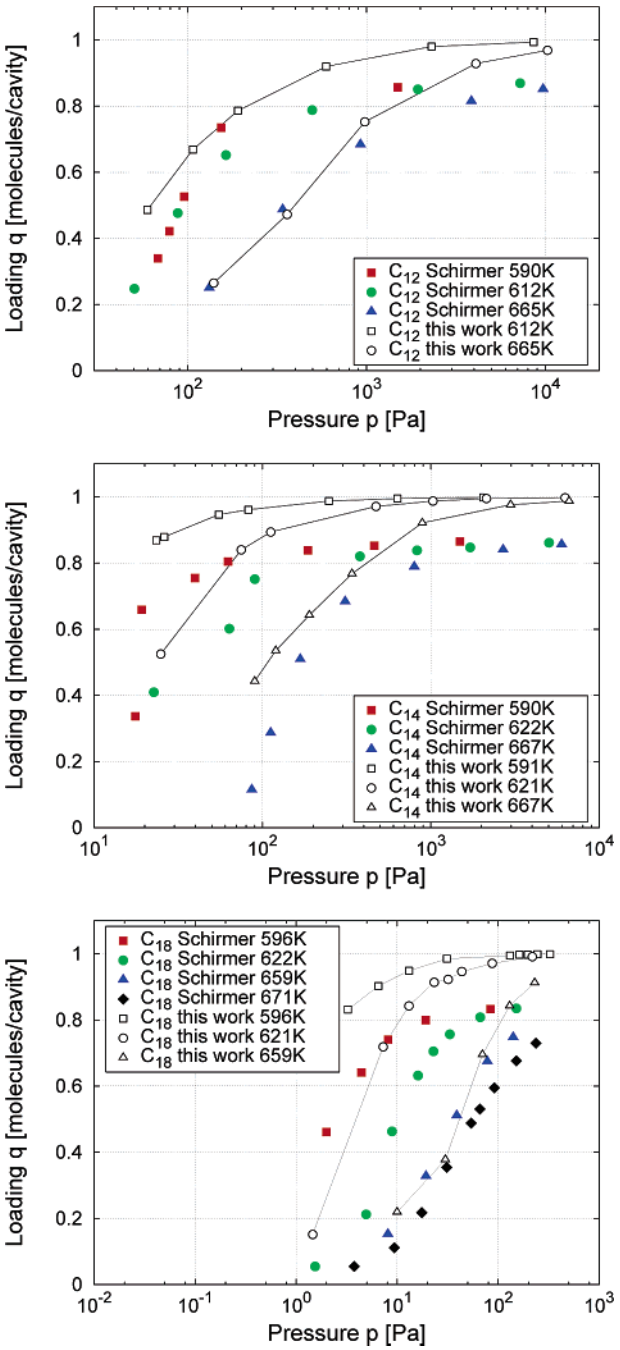

Figure 4. Predictions for long alkanes: C_{12}, C_{14} and C_{18} at various temperatures in Ca/Na-LTA compared to experimental data of Schirmer.

As can be seen, adsorption increases with the *amount* of ions present in the α-cages of LTA 5A. The amount is more important than the type of ions. LTA 4A with 96 sodium ions would show very high adsorption capacity, but unfortunately also have all the eight-ring windows blocked. Methane and ethane would diffuse at acceptable rates (for practical purposes), but the diffusivities of longer alkanes are very low. Experimental data on LTA 4A are scattered and almost impossible to determine for the longest alkanes due to the excessively long equilibration times. Here, we show that also for LTA5A much of the scatter can be explained by differences in the Ca/Na ratio and, therefore, in the amount of ions present. The Ca/Na ratio influences not only adsorption properties, but also diffusion and equilibration times.

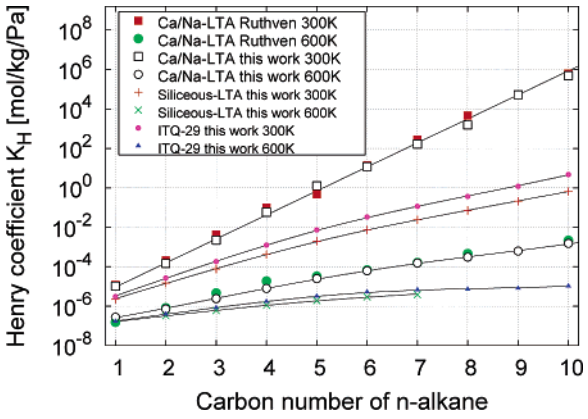

Figure 5. Henry coefficients for the Ca/Na form and siliceous LTA form obtained from simulation compared to experimental data of Ruthven et al. as a function of chain length at 300 K and 600 K. At low pressures, the loading is linear in the pressure with the Henry coefficient as the proportionality constant.

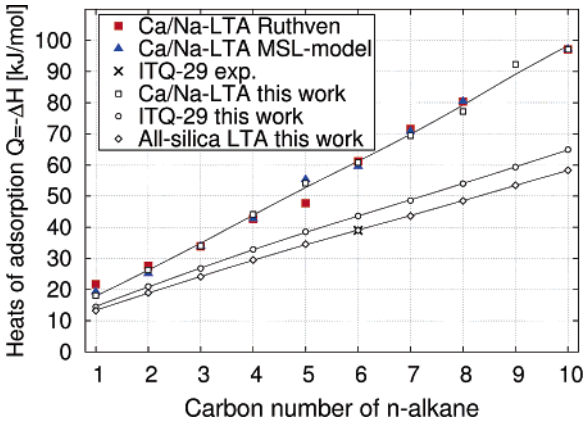

Figure 6. Heats of adsorption for the Ca/Na form and siliceous LTA form obtained from simulation compared to experimental data of Ruthven et al. as a function of chain length.

TABLE 4: Comparison of Our Simulations Results of Low-Coverage Properties in Ca/Na-LTA with the Experimental Results of Ruthven et al.[a]

	K_∞ [mol/kg/Pa]		$-\Delta H$ [kJ/mol]	
CN	sim	exptl	sim	exptl
1	1.5×10^{-8}	1.9×10^{-9}	16.7	21.8
2	3.7×10^{-9}	3.3×10^{-9}	26.3	27.6
3	2.8×10^{-9}	5.2×10^{-9}	33.9	33.9
4	1.1×10^{-9}	3.6×10^{-9}	44.2	42.7
5	4.4×10^{-10}	2.3×10^{-9}	54.1	47.7
6	3.2×10^{-10}	3.2×10^{-10}	60.8	61.1
7	1.4×10^{-10}	9.5×10^{-11}	69.4	71.6
8	5.6×10^{-11}	4.7×10^{-11}	77.2	80.4
9	6.3×10^{-12}		91.3	
10	4.0×10^{-12}	7.6×10^{-12}	97.1	97.1

[a] Both the Ruthven and the simulation henry coefficients K_H of the linear alkanes have been fitted to $K_H = K_\infty e^{(-\Delta H/RT)}$ in the temperature range $T = 300-600$ K. Here, K_∞ denotes the pre-exponential Henry coefficient, ΔH the enthalpy of adsorption, and $R = 8.31451$ J/mol/K the gas constant.

IV. Conclusions

We have calibrated a new force field for Ca/Na-aluminosilicates applicable over a wide range of Si/Al ratios. The calibration set was the data of Ruthven for methane, ethane, and propane. The predicted isotherms show good agreement with other experimental isotherms although the scatter in the experimental data is large. The predicted heats of adsorption

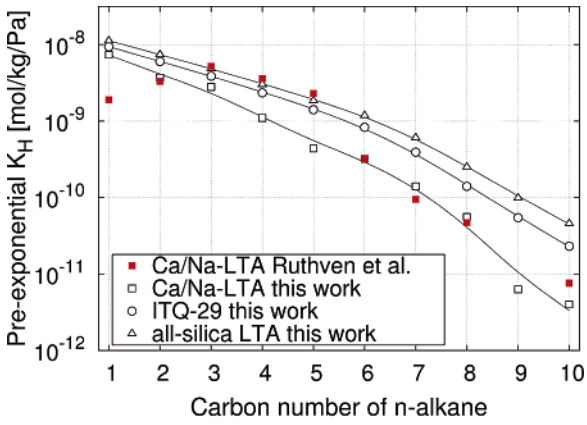

Figure 7. Preexponential Henry coefficients in log scale for the Ca/Na form, ITQ-29 siliceous LTA form obtained from simulation, and experimental data on Ca/Na-LTA of Ruthven et al. as a function of chain length.

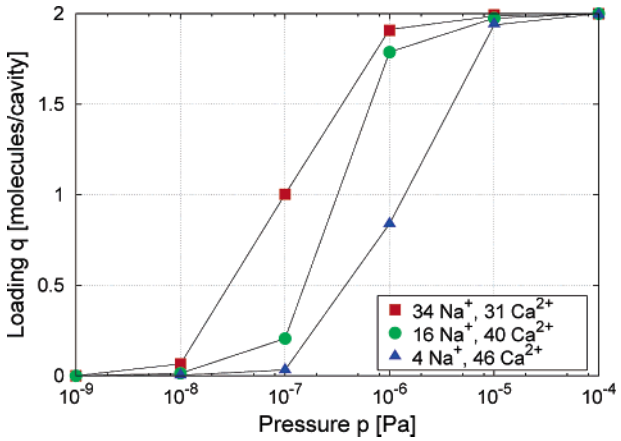

Figure 8. Influence of the Ca/Na ratio on adsorption of decane in LTA 5A at 300 K. Adsorption increases with the amount of ions present in the α-cages. LTA 4A has 96 Na ions and would have a very high adsorption capacity, but in LTA 4A, all eight-ring windows are blocked, rendering it practically useless for alkane adsorption.

and Henry coefficient show almost perfect agreement. In addition to zeolite 5A, we also computed the heats of adsorption and Henry coefficients for the newly synthesized LTA-type silica. The only experimental data point for the heat of adsorption was in very good agreement with the value computed for this silica. Simulation and experimental data present differences in the Na/Ca ratios and in the equilibration times that can possibly explain the discrepancies between simulations and experiment, and between experimental datasets.

Acknowledgment. This work is supported by the Spanish "Ministerio de Educacíon y Ciencia" (Ramón y Cajal Program and projects CTQ2004-00582/BQU, CTQ2004-07730-C02-01/BQU, VEM2003 20574 C03 01) and by the Dutch STW/CW program Separation Technology (700.56.655-DPC.6243) and by the National Science Foundation (CTS-0507013). We thank R. Krishna and R. Q. Snurr for useful discussions and comments on the manuscript. E.G.-P. wishes to thank the MEC for a grant to prepare her Doctoral work.

References and Notes

(1) Corma, A.; Rey, F.; Rius, J.; Sabater, M. J.; Valencia, S. *Nature (London)* **2004**, *431*, 287−290.

(2) Kaerger, J.; Ruthven, D. M. *Diffusion in Zeolites and other Microporous Solids*; John Wiley & Sons: New York, 1992.

(3) Jobic, H.; Karger, J.; Krause, C.; Brandani, S.; Gunadi, A.; Methivier, A.; Ehlers, G.; Farago, B.; Haeussler, W.; Ruthven, D. M. *Adsorption* **2005**, *11*, 403−407.

(4) Fritzsche, S.; Haberlandt, R.; Kärger, J.; Pfeifer, H.; Waldherrteschner, M. *Stud. Surf. Sci. Catal.* **1994**, *84*, 2139−2146.

(5) Fritzsche, S.; Gaub, M.; Haberlandt, R.; Hofmann, G. *J. Mol. Model.* **1996**, *2*, 286−292.

(6) Fritzsche, S.; Wolfsberg, M.; Haberlandt, R.; Demontis, P.; Suffritti, G. B.; Tilocca, A. *Chem. Phys. Lett.* **1998**, *296*, 253−258.

(7) Fritszche, S.; Haberlandt, R.; Wolfsberg, M. *Chem. Phys.* **2000**, *253*, 283−294.

(8) Bates, S. P.; van Well, W. J. M.; van Santen, R. A.; Smit, B. *J. Am. Chem. Soc.* **1996**, *118*, 6753−6759.

(9) Demontis, P.; Suffritti, G. B. *J. Phys. Chem. B* **1997**, *101*, 5789−5793.

(10) Haberlandt, R. *Thin Solid Films* **1998**, *330*, 34−45.

(11) Murashov, V. V. *J. Phys.: Condend. Matter* **1999**, *11*, 1261−1271.

(12) Schüring, A.; Auerbach, S. M.; Fritzsche, S.; Haberlandt, R. *J. Chem. Phys*. **2002**, *116*, 10890−10894.

(13) Schüring, A.; Auerbach, S. M.; Fritzsche, S.; Haberlandt, R. *Stud. Surf. Sci. Catal.* **2004**, *154*, 2110−211.

(14) Dubbeldam, D.; Calero, S.; Maesen, T. L. M.; Smit, B. *Phys. Rev. Lett.* **2003**, *90*, 245901.

(15) Dubbeldam, D.; Smit, B. *J. Phys. Chem. B* **2003**, *107*, 12138−12152.

(16) Tunca, C.; Ford, D. M. *J. Chem. Phys.* **1999**, *111*, 2751−2760.

(17) Tunca, C.; Ford, D. M. *J. Phys. Chem. B* **2002**, *106*, 10982−10990.

(18) Tunca, C.; Ford, D. M. *Chem. Eng. Sci.* **2003**, *58*, 3373−3383.

(19) Beerdsen, E.; Smit, B.; Dubbeldam, D. *Phys. Rev. Lett.* **2004**, *93*, 248301.

(20) Dubbeldam, D.; Beerdsen, E.; Vlugt, T. J. H.; Smit, B. *J. Chem. Phys.* **2005**, *122*, 224712.

(21) Beerdsen, D. Dubbeldam E.; Calero, S.; Smit, B. *J. Phys. Chem. B* **2006**, *110*, 3164−3172.

(22) Demontis, P.; Fenu, L. A.; Suffritti, G. B. *J. Phys. Chem. B* **2005**, *109*, 18081−18087.

(23) Beerdsen, E.; Dubbeldam, D.; Smit, B. *Phys. Rev. Lett.* **2006**, *96*, 044501.

(24) Jaramillo, E.; Chandross, M. *J. Phys. Chem. B* **2004**, *108*, 20155−20159.

(25) Calero, S.; Dubbeldam, D.; Krishna, R.; Smit, B.; Vlugt, T. J. H.; Denayer, J. F. M.; Martens, J. A.; Maesen, T. L. M. *J. Am. Chem. Soc.* **2004**, *126*, 11377−11386.

(26) Dubbeldam, D.; Calero, S.; Vlugt, T. J. H.; Krishna, R.; Maesen, T. L. M.; Beerdsen, E.; Smit, B. *Phys. Rev. Lett.* **2004**, *93*, 088302-1.

(27) Dubbeldam, D.; Calero, S.; Vlugt, T. J. H.; Krishna, R.; Maesen, T. L. M.; Smit, B. *J. Phys. Chem. B* **2004**, *108*, 12301−12313.

(28) Martin, M. G.; Siepmann, J. I. *J. Phys. Chem. B* **1999**, *103*, 4508−4517.

(29) Martin, M. G.; Thompson, A. P.; Nenoff, T. M. *J. Chem. Phys.* **2001**, *114*, 7174−7181.

(30) Bezus, A. G.; Kiselev, A. V.; Lopatkin, A. A.; Du, P. Q. J. *J. Chem. Soc., Faraday Trans. 2* **1978**, *74*, 367−379.

(31) Beerdsen, E.; Smit, B.; Calero, S. *J. Phys. Chem. B* **2002**, *106*, 10659−10667.

(32) Beerdsen, E.; Dubbeldam, D.; Smit, B.; Vlugt, T. J. H.; Calero, S. *J. Phys. Chem. B* **2003**, *107*, 12088−12096.

(33) Calero, S.; Lobato, M. D.; García-Pérez, E.; Mejías, J. A.; Lago, S.; Vlugt, T. J. H.; Maesen, T. L. M.; Smit, B.; Dubbeldam, D. *J. Phys. Chem. B.* **2006**, *110*, 5838-5841.

(34) Jaramillo, E.; Auerbach, S. M. *J. Phys. Chem. B* **1999**, *103*, 9589−9594.

(35) Garcia-Perez, E.; Torrens, I. M.; Lago, S.; Dubbeldam, D.; Vlugt, T. J. H.; Smit, B.; Krishna, R.; Calero, S. *Appl. Surf. Sci.* **2005**, *252*, 716−722.

(36) Garcia-Perez, E.; Torrens, I. M.; Lago, S.; Krishna, R.; Smit, B.; Calero, S. *Stud. Surf. Sci. Catal. Parts A−B* **2005**, *158*, 1097−1104.

(37) Liu, B.; Smit, B. *Phys. Chem. Chem. Phys.* **2006**, *8*, 1852−1857.

(38) Macedonia, M. D.; Maginn, E. *J. Mol. Phys.* **1999**, *96*, 1375−1390.

(39) June, R. L.; Bell, A. T.; Theodorou, D. N. *J. Phys. Chem.* **1992**, *96*, 1051−1060.

(40) Pascual, P.; Ungerer, P.; Tavitian, B.; Pernot, P.; Boutin, A. *Phys. Chem. Chem. Phys.* **2003**, *5*, 3684−3693.

(41) Vlugt, T. J. H.; Krishna, R.; Smit, B. *J. Phys. Chem. B* **1999**, *103*, 1102−1118.

(42) Smit, B.; Loyens, L. D. J. C.; Verbist, G. L. M. M. *Faraday Discuss.* **1997**, *106*, 93−104.

(43) Pluth, J. J.; Smith, J. V. *Zeolites* **1980**, *102*, 4704−4708.

(44) Kerr, G. T. *Inorg. Chem.* **1966**, *5*, 1537−1539.

(45) Allen, M. P.; Tildesley, D. J. *Computer Simulation of Liquids*; Clarendon Press: Oxford, 1987.

(46) Frenkel, D.; Smit, B. *Understanding Molecular Simulation*, 2nd ed.; Academic Press: London, 2002.
(47) Ryckaert, J. P.; Bellemans, A. *Faraday Dicuss. Chem. Soc.* **1978**, *66*, 95−106.
(48) Kiselev, A. V.; Lopatkin, A. A.; Shulga, A. A. *Zeolites* **1985**, *5*, 261−267.
(49) Vlugt, T. J. H.; Schenk, M. *J. Phys. Chem. B* **2002**, *106*, 12757−12763.
(50) Smit, B.; Maesen, T. L. M. *Nature* **1995**, *374*, 42−44.
(51) Smit, B.; Siepmann, J. I. *J. Phys. Chem.* **1994**, *98*, 8442−8452.
(52) Pluth, J. J.; Smith, J. V. *J. Am. Chem. Soc.* **1980**, *102*, 4707−4708.
(53) Schirmer, W.; Fiedrich, G.; Grossmann, A.; Stach, H., In *Molecular Sieves*; Proc. 1st International Conference on Zeolites; Society of Chemical Industry: London, 1968; p 276.
(54) Firor, R. L.; Seff, K. J. *J. Am. Chem. Soc.* **1978**, *100*, 3091−3096.
(55) Moon, G. K.; Choi, S. G.; Lee, S. H. *Bull. Korean Chem. Soc.* **1993**, *14*, 356−362.
(56) Jang, S. B. *Korean J. Cryst.* **1990**, *1*, 76.
(57) Pluth, J. J.; Smith, J. V. *J. Am. Chem. Soc.* **1983**, *105*, 1192−1195.
(58) Adams, J. M.; Haselden, D. A. *J. Solid. State Chem.* **1984**, *51*, 83−90.
(59) Ruthven, D. M.; Loughlin, K. F. *J. Chem. Soc., Faraday Trans. 1* **1972**, *68*, 696.
(60) Ruthven, D. M. *AIChe J.* **1976**, *22*, 753−759.
(61) Loughlin, K. F.; Hasanain, M. A.; AbdulRehman, H. B. *Ind. Eng. Chem. Res.* **1990**, *29*, 1535−1546.
(62) Ruthven, D. M.; Derrah, R. I. *Can. J. Chem. Eng.* **1992**, *50*, 743−747.
(63) Ruthven, D. M.; Loughlin, K. F. *Chem. Eng. Sci.* **1971**, *26*, 1145.
(64) Silva, J. A. C.; Rodrigues, A. E. *Ind. Eng. Chem. Res.* **1997**, *36*, 493−500.
(65) Silva, J. A. C.; Rodrigues, A. E. *AIChe J.* **1997**, *43*, 2524−2534.
(66) Doetsch, I. H.; Ruthven, D. M.; Loughlin, K. F. *Can. J. Chem.* **1974**, *52*, 2717−2724.
(67) Vavlitis, A. P.; Ruthven, D. M.; Loughlin, K. F. *J. Colloid Interface Sci.* **1981**, *84*, 526−531.
(68) Miano, F. *Colloids Surf. A* **1996**, *110*, 95−104.